Formation of CO in the Reaction of Oxygen Atoms with CH_3: Reaction over a Barrier but Not through a Saddle Point

Vadim D. Knyazev

Research Center for Chemical Kinetics, Department of Chemistry, The Catholic University of America, Washington, D.C., 20064, and National Institute of Standards and Technology, Physical and Chemical Properties Division, Gaithersburg, Maryland 20899

Received: February 7, 2002; In Final Form: June 17, 2002

A type of chemical reaction characterized by a reaction path proceeding over an energy barrier (a ridge of the potential energy surface) but not through a saddle point is described. A method of computation of rate constants for such "over-the-ridge" reactions is developed on the basis of RRKM and transition state theories. Formulas and computational procedures are presented for the cases of microscopic energy-dependent rates of unimolecular reactions and the thermally averaged rates of unimolecular or bimolecular reactions. This method is applied to compute the branching fraction of the CO-producing channel (channel 1c) of the reaction of O atoms with CH_3 radicals. A quantum chemical computational study of the potential energy surface (PES) of the decomposition of CH_3O was performed using UHF, UMP2, QCISD, and B3LYP methods as well as single-point G2 and CBS-Q energy calculations. The results demonstrate that the products of the reaction channel 1c are formed in a process characterized by trajectories in coordinate space that proceed over a potential energy ridge but not through a saddle point. The method developed in this work was used to calculate the microscopic energy-dependent rate constants of the decomposition of CH_3O and the branching fraction of the CO-producing reaction channel (1c). The calculated values of the channel 1c fraction, 4−7% (depending on the potential energy surface used), although lower than the experimental values, overlap in their range of uncertainties with the experiments at the lower end (15 ± 3% and 18 ± 4%) of the reported scope of the experimental results which range from 15 ± 3% to 40 ± 10%.

I. Introduction

Traditionally, the exploration of mechanisms of reactions and, consequently, the computation of related rate parameters have concentrated on identifying and studying properties of saddle points on potential energy surfaces (PES) of reactive systems. This predominant attention to PES saddle points is based on two paradigmatic postulations. First is the identification of the minimum energy path connecting the reactants and the products of a particular reaction channel with the reaction coordinate. The reaction coordinate itself can be defined conceptually and mathematically in different ways but it is generally associated with the length along the intuitive "reaction path" describing the transformation of the reactive system in its motion from reactants to products. The second assumption is that this minimum energy path, at least in the vicinity of the energy barrier, represents a local minimum of PES in all directions (degrees of freedom) except for the one that corresponds to the "reaction coordinate," thus forming a valley on the PES. If an energy barrier is present, then this valley path, crossing over the barrier, necessarily passes through a PES saddle point. This second assumption is usually taken as self-evident and thus avoids discussion. One exception is the issue of reaction path bifurcations, such as those occurring at valley-ridge inflection points, which has received significant attention (e.g., refs 1−7). The local minimum/valley/saddle point assumption is correct for the lowest energy channel but is not necessarily valid for the higher energy channels. For the lowest energy channel, any trajectory adjacent (in coordinate space) to that passing through a saddle point proceeds to the same products but over a slightly higher energy barrier. One can, however, imagine a system where two adjacent trajectories that pass over the energy barrier (separating the reactant and the product valleys) in the vicinity of a bifurcation point proceed to different product sets. This situation is illustrated in Figure 1. Figure 1a depicts a "traditional" reactive system with two channels, each characterized by its corresponding saddle point (TS1 and TS2). Figure 1b presents a reactive system where only the lowest energy channel has an associated saddle point. The bifurcation point on the potential energy surface "ridge" is shown by the vertical line. Trajectories that pass over the ridge to the left of this line proceed to the products of the second channel while those that cross the PES ridge on the right side of this bifurcation point are a part of the reaction flux representing the first, lowest energy, reaction channel.

Such reaction channels that proceed over PES ridges but have no associated saddle points have received little attention in terms of methods of theoretical modeling. To the best of the author's knowledge, statistical theories of chemical reactions have not been applied to such situations. Although reaction modeling based on the use of classical and quasi-classical trajectory methods is capable of detecting and quantifying such reaction channels, no studies have specifically concentrated on this "over-the-ridge" type of reactions. This lack of attention is partially explained by the fact that such "reactions without saddle points" are not the lowest energy channels. The vast majority of experimental studies of elementary chemical reactions are conducted at low and moderate temperatures where the steep decline of the Boltzmann distribution with energy ensures that, in thermally activated cases, only the lowest energy channels

10.1021/jp020366t CCC: $22.00
Published on Web 08/17/2002

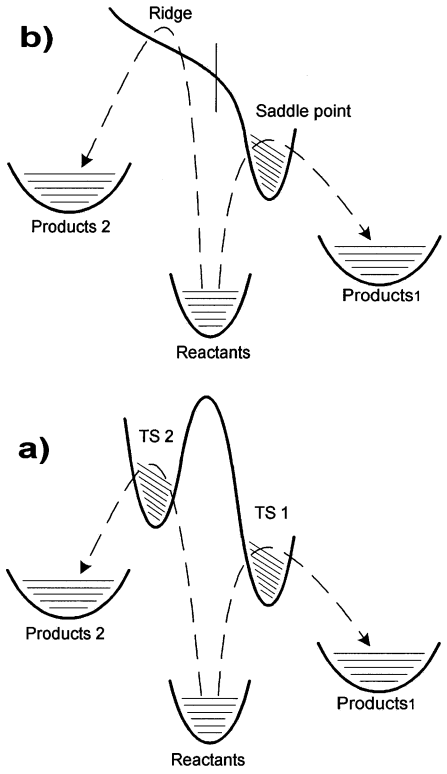

Figure 1. Qualitative character of the potential energy surface for reactions proceeding over an energy barrier but not through PES saddle points. (a) A "traditional" reactive system with two channels each characterized by its corresponding saddle point (TS1 and TS2). (b) A reactive system where only the lowest energy channel has an associated saddle point. The bifurcation point on the potential energy surface "ridge" is shown by the vertical line. Trajectories that pass over the ridge to the left of this line proceed to the products of the second channel while those that cross the PES ridge on the right side of this bifurcation point are part of the reaction flux representing the first, lowest energy, reaction channel.

are important. The situation, however, is different for chemically activated reactions where the initial energy distribution is often positioned at high energies and the competition between reaction channels includes channels with very different energy barriers as contestants. The recently reinvigorated attention to accurate computational description of the pressure and temperature dependences of the kinetics of chemically activated reactions calls for the development of methods of describing reaction channels proceeding over energy barriers (PES ridges) but not through saddle points.

This article[8] presents an RRKM-theory[9−12] based method to calculate the microscopic energy-dependent rate constants of a unimolecular reaction channel without a saddle point. The technique is demonstrated by its application to the channel of formation of CO in the reaction of O atoms with CH_3 radicals.

The reaction of oxygen atoms with methyl radical

$$O + CH_3 \rightarrow \text{products} \qquad (1)$$

is an important part of the complex mechanism of combustion of hydrocarbon fuels.[13−15] Due to the relative inefficiency of the high-temperature reaction between CH_3 and O_2 (equilibrium in the addition step is shifted to the CH_3+O_2 side), reaction 1 is the major channel of removal of methyl radicals under lean fuel conditions.[13−15] Several experimental studies (refs 16−23, also see reviews in refs 24 and 25) resulted in an overall rate constant 1.4×10^{-10} cm^3 molecule^{-1} s^{-1}, independent of temperature. The widest temperature range was covered in the experiments of Slagle et al.[19] who isolated reaction 1 for direct study by the laser photolysis/photoionization mass spectrometry (LP/PIMS) technique between 294 and 900 K at low pressures.

It has been generally assumed that the only channel of reaction 1 is that producing formaldehyde (detected in several of the above experimental studies) and hydrogen atom:

$$O + CH_3 \rightarrow CH_2O + H \qquad (\Delta H^0_{298} = -286 \text{ kJ mol}^{-1}) \qquad (1a)$$

In 1992 Seakins and Leone[26] detected the formation of vibrationally excited CO in their room-temperature laser photolysis/FTIR emission study of reaction 1, thus providing experimental evidence for the existence of a second channel

$$O + CH_3 \rightarrow H + CO + H_2 \qquad (\Delta H^0_{298} = -288 \text{ kJ mol}^{-1}) \quad (1b)$$

Seakins and Leone obtained the distribution of vibrational levels of the CO molecule formed in reaction 1b from fitting calculated emission intensities to a low-resolution (2 cm^{-1}) experimentally obtained FTIR emission spectrum. This analysis resulted in a CO vibrational temperature of 12700 ± 1400 K.

Recent laser photolysis/laser-induced fluorescence experiments of Min et al.[27] have confirmed the formation of excited CO in reaction 1, providing, however, a significantly lower degree of CO vibrational excitation, that corresponding to a vibrational temperature of about 2000 K. In ref 27, the populations of the vibrational levels $v = 0$ and $v = 1$ were obtained by comparing the fluorescence signals with those obtained from the CO photoproduct of acetone photolysis and the ratio of $v = 2$ to $v = 0$ populations was obtained from the direct comparison of fluorescence signals.

Both the studies of Seakins and Leone[26] and Min et al.[27] were conducted at room temperature and similar low pressures: 36−600 Pa (0.3−4.5 Torr)[26] and 27 Pa (0.2 Torr).[27] The reasons for the substantial disagreement in the degrees of vibrational excitation of the CO product of reaction 1b are unknown.

The values of the reaction channel 1b branching ratio were reported by several groups. Seakins and Leone obtained 40 ± 10% branching fraction for CO formation by comparing the IR emission signal intensities of several of the lowest vibrational levels of CO obtained in reaction 1b with those of CO originating from the acetone photolysis. In these experiments, 193 nm photolysis of acetone was used as the source of CH_3 radicals, and thus, CO concentrations obtained in the photolysis provided the measure of the initial CH_3 concentrations. This value of the branching ratio was dependent on the CO vibrational excitation distribution obtained by the same authors (see above). In 1999, Fockenberg et al.[23] studied reaction 1 at room temperature and 133 Pa (1 Torr) using the LP/PIMS technique with a time-of-flight mass spectrometer. These authors reported 17 ± 11% branching fraction for reaction channel 1b. In a subsequent work by Preses et al.,[28] this value was refined (18 ± 4%) by using diode laser absorption experiments with isotopically substituted acetone as a source of CH_3 radicals and reference concentrations of ^{13}CO. Slagle et al.[29] used the LP/PIMS method to determine the branching fraction of reaction channel 1a by monitoring the formation of formaldehyde, the major product of reaction 1. The reported value of channel 1a branching fraction, 85 ± 15%, results in the 0−30% range of possible values of the fraction of the CO-producing channel 1b. Finally, Fockenberg[30] reported an expanded version of the earlier LP/PIMS study where the temperature-independent value of 15 ± 3% was reported for the channel 1b fraction.

Despite the experimentally proven importance of the CO-producing reaction channel 1b, theoretical attempts to locate a corresponding transition state have failed.[29] The initial act of reaction 1 is believed to be the addition of O atom to the CH_3 radical with the formation of a highly vibrationally excited CH_3O radical ($\Delta H^0_{298} = -378$ kJ mol^{-1}). This excited radical subsequently undergoes rapid decomposition to products via a chemically activated mechanism. Collisional stabilization is not expected to be important under any experimentally achievable conditions due to the very large decomposition rates. The reaction pathway corresponding to channel 1a is that of simple H elimination from CH_3O (the reaction energy barrier is likely to be in the 107−143 kJ mol^{-1} range, see review in ref 26). The most plausible pathway resulting in the formation of CO is the initial elimination of H_2

$$O + CH_3 \rightarrow CH_3O^* \rightarrow H_2 + HCO \qquad (\Delta H^0_{298} = -354 \text{ kJ mol}^{-1}) \quad (1c)$$

Since reaction channel 1c leaves 354 kJ mol^{-1} to be distributed among the two products and the C−H bond of HCO is only 70 kJ mol^{-1},[31,32] channel 1c, most likely, will be followed by the immediate decomposition of excited HCO producing H and CO

$$HCO^* \rightarrow H + CO \qquad (2)$$

In the theoretical part of the study of Slagle et al.,[29] attempts were made to locate a transition state (PES saddle point) that would lead to the products of reaction channels 1b or 1c. None, however, could be found. As will be demonstrated in this article, analysis of the PES strongly suggests that formation of the H_2 + HCO products in the O + CH_3 reaction occurs without participation of a PES saddle point connecting the reactants with the products. Instead, reaction channel 1c (which will lead, via reaction 2, to the final products of channel 1b, H_2 + H + CO) proceeds through the area on the PES that involves crossing over an energy barrier (PES "ridge") but has no associated saddle point. Since the study of reaction 1 in this article is mostly concerned with the transformations of the excited CH_3O adduct, the following reaction channel numbering will also be used:

$$CH_3O \rightarrow H + H_2CO \qquad (3a)$$

$$CH_3O \rightarrow H_2 + HCO \qquad (3b)$$

This article is organized as follows. Following this introduction, the method of computing microscopic energy-dependent rate constants $k(E)$ for unimolecular reactions proceeding over energy barriers (PES ridges) but not through saddle points is presented in section II. An ab initio study of the potential energy surface of reaction 1 (reaction channels 3a and 3b) is presented in section III. Application of the $k(E)$ computation method to reaction 3 (and, consequently, reaction 1) is described in section IV where the branching fraction of the reaction channel 1c (or 1b) is calculated and the uncertainties of the model are investigated. A discussion is presented in section V. Finally, a summary of the results is given in section VI.

II. Method

II.1. Energy Specific Rate Constants of Unimolecular Reactions. This subsection presents a general method of computing microscopic energy-dependent rate constants $k(E)$ for unimolecular reactions proceeding over energy barriers (PES ridges) but not necessarily through PES saddle points. The method is based on the formalism of the RRKM theory, which is a microcanonical (energy or energy-and-angular-momentum specific) version of transition state theory (see refs 9−12 for comprehensive descriptions of RRKM theory). In this work, only the energy-specific formalism is considered. In the RRKM method, a surface separating the reactants and the products is identified in the phase space of the reactive system. In most practical implementations of the RRKM method for reactions with identifiable barriers, this dividing surface is positioned in the coordinate subspace of the phase space, i.e., all trajectories crossing this surface in the correct direction are assumed to have passed from reactants to products regardless of their corresponding momentum components.

The RRKM expression for the microscopic energy-dependent rate constant

$$k(E) = \frac{W^{\neq}(E - E_0)}{h\rho(E)} \qquad \text{(I)}$$

(here $W^{\neq}(E)$ is the sum of states of the transition state, $\rho(E)$ is the density of states of the active molecule, and E_0 is the reaction energy barrier) can be derived classically by counting the number of trajectories originating in the reactants' subspace and crossing the dividing surface. This counting is performed by integrating over the phase space (see, for example, formula 3.5.5 of ref 9):

$$k(E) = \frac{\int_0^{E-E_0} d\epsilon \int d\Gamma_u \delta[H_u - (E - E_0 - \epsilon)]}{\int d\Gamma\, \delta[H - E]} \qquad \text{(II)}$$

where E is energy, $d\Gamma$ is an element of phase space, H denotes the Hamiltonian, and the subscript "u" signifies that $d\Gamma_u$ and H_u represent the phase space element and the Hamiltonian of the dividing surface, respectively. From expression II follows the additivity of the microscopic rates $k(E)$ with respect to the dividing surface, i.e., if the dividing surface is artificially separated into two parts (designated as part 1 and part 2), then, due to the additivity of integration,

$$k(E) = k_1(E) + k_2(E) \qquad \text{(III)}$$

where $k_1(E)$ and $k_2(E)$ are computed for the first and the second parts of the dividing surface, respectively. The same is achieved by

$$W^{\neq}(E) = W^{\neq}_1(E) + W^{\neq}_2(E) \qquad \text{(IV)}$$

since $\rho(E)$ is the same for both parts 1 and 2.

Dividing Surface. The first step in the calculation of the rate constants is the identification of the dividing surface. Intuitively, it seems natural to position the dividing surface in the coordinate space along the PES ridge separating the reactants and the products. The exact definition of the ridge, however, is not unambiguous. In this study, one method of defining this separating ridge is proposed, as follows.

At a given point $\mathbf{x_0}$ in coordinate space (coordinates are mass-weighted), let us expand the PES in harmonic terms by diagonalizing the projected force constant matrix (i.e., the matrix from which the translational degrees of freedom, overall rotations, and motion along the PES gradient are projected out[33]) and presenting the potential energy V in the form

$$V(s,\xi) = V_0(s) + \sum_{k=1}^{N-1} {}^1/_2\, \lambda_k \xi_k^2 \qquad \text{(V)}$$

where s is the coordinate along the PES gradient, λ_k and ξ_k are the eigenvalues of the projected matrix and the associated normal coordinates, and N is the number of internal degrees of freedom ($N - 1$ normal modes indexed by k and one more degree of freedom associated with the motion along the PES gradient). The point $\mathbf{x_0}$ is considered to be on the separating ridge of the PES if the following two conditions are satisfied:

(1) One (and only one) of the eigenvalues of the projected force constant matrix is negative. We will assign to it the index $k = 1$ and denote the corresponding normal coordinate vector $\mathbf{e_1}$.

(2) The steepest descent paths (SDP)[34] started at points $\mathbf{x_1}$ and $\mathbf{x_2}$ given by $\mathbf{x_{1,2}} = \mathbf{x_0} \pm \mathbf{e_1}\delta\xi_1$ lead to the reactants and products, respectively (here, $\delta\xi_1$ is a small increment of the ξ_1 normal coordinate).

If condition 2 is satisfied for any small $\delta\xi_1$, then the steepest descent path originating in $\mathbf{x_0}$ can be expected to run along the thus defined ridge and to be unstable (i.e., any minor displacement to either side of the ridge will lead the SDP away from the ridge, to reactants or products).

We will now approximate the reaction dividing surface positioned on the PES ridge by a combination of the degree of freedom associated with the motion along the PES ridge (coordinate s) and the $N - 2$ degrees of freedom associated with the ξ_k (k ranging from 2 to $N - 1$) normal coordinates at each point along the ridge. The ξ_1 coordinate orthogonal to the dividing surface is thus associated with the motion of the reactive system from reactants to products and represents the reaction coordinate.

The above method of defining the PES ridge and the reaction dividing surface is not unique. One can mention, for example, potential methods of analyzing PES ridges based on following gradient extremals,[6,35−38] which, generally, differ from the SDPs. The formalism presented below is valid provided that, in addition to the usual assumptions of the RRKM theory (see, for example, refs 9−12), one can identify one degree of freedom on the dividing surface that corresponds to motion along the PES ridge and the Hamiltonian of this degree of freedom is separable from that of the rest of the degrees of freedom at each point along the ridge.

Rate Constants. The dividing surface can be considered as a pseudo-molecule ("transition state") which has N-1 degrees of freedom. In the next step, we separate the degree of freedom of this dividing surface that corresponds to the motion along the PES ridge from the remaining $N - 2$ degrees of freedom. We assign coordinate q to this motion along the PES ridge (q may coincide with the s coordinate used above in the proposed definition of the PES ridge but is more general as it is not restricted to a mass weighted coordinate system and to this particular method of defining the dividing surface). If the above condition of separability of the motion along the PES ridge from the rest of the degrees of freedom is satisfied, the transition state sum of states (obtained by taking the integral in the numerator of expression II over the dividing surface) can be expressed via the convolution formula[9]

$$W^{\neq}(E) = \int_0^E \mathrm{d}\epsilon \rho_1(\epsilon) W_2(E-\epsilon) \qquad \text{(VI)}$$

Here, $\rho_1(\epsilon)$ is the density-of-states function of the degree of freedom corresponding to the motion along the PES ridge and $W_2(\epsilon)$ is the sum-of-states function of the pseudo-molecule "consisting" of the remaining $N - 2$ degrees of freedom.

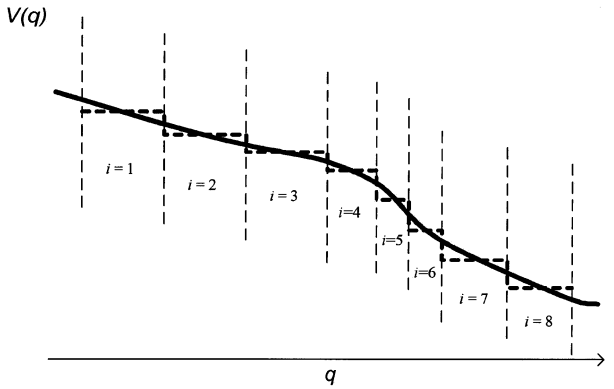

Figure 2. Representation of the reaction dividing surface with a sequence of segments (indexed by i) obtained by "cutting" at selected values of q. Vertical dashed lines separate the segments. Solid line: $V(q)$ potential energy function along the PES ridge. Heavy dashed line: representation of $V(q)$ with a series of "flat" steps of energy E_i corresponding to the individual segments.

The density-of-states of the motion along the PES ridge (with coordinate q) can be calculated classically using the formula[39]

$$\rho_1(E) = \frac{1}{\sqrt{B}} \int_0^E \frac{\tilde{\rho}_{\mathrm{SH}}(\epsilon)\, \mathrm{d}\epsilon}{\sqrt{E-\epsilon}} \qquad \text{(VII)}$$

where the "shape-related"[39] density-of-states function

$$\tilde{\rho}_{\mathrm{SH}}(E) = \frac{1}{2\pi} \frac{\mathrm{d}w(E)}{\mathrm{d}E} \qquad \text{(VIII)}$$

is expressed via the derivative of the "width" ($w(E)$) of the potential energy function, i.e., the distance (in terms of the reduced coordinate q/q_0, q_0 being an arbitrarily fixed value) between the "walls" of the potential energy function at a particular energy E. Here, B is the effective rotational constant of the associated "pseudo-rotation"[39] (μ is the reduced mass):

$$B = \frac{h^2}{8\pi^2 \mu q_0^{\,2}} \qquad \text{(IX)}$$

The reader is referred to ref 39 for details of the definitions and formalism of the treatment of densities of states of nonharmonic degrees of freedom (including the origin and the definition of the term "pseudo-rotation") used in the current derivation.

As one moves along the PES ridge, the properties (vibrational frequencies and geometry) of the pseudo-molecule can change quite significantly, thus affecting the value of $W_2(\epsilon)$. This change can be taken into account by using the additivity property discussed above (expressions III and IV). The dividing surface can be subdivided into segments by "cutting" it at selected values of q (Figure 2). $W_2(E)$ is then calculated separately for each segment with the dependence of the molecular properties along the ridge coordinate q taken into account and the overall sum-of-states function is obtained by summing over all segments (indexed by i):

$$W^{\neq}(E) = \sum_i \int_0^E d\epsilon \rho_{1,i}(\epsilon) W_{2,i}(E-\epsilon) \qquad \text{(X)}$$

For practical implementations of this method, it may be convenient to approximate the actual potential energy function along the PES ridge, $V(q)$, with a series of "flat" steps of energy

E_i and width Δq corresponding to the individual segments. Then

$$\tilde{\rho}_{SH}(E) = \frac{\Delta q}{2\pi q_0}\,\delta(\epsilon - E_i) \qquad \text{(XI)}$$

and

$$\rho_1(E) = \frac{1}{\sqrt{\tilde{B}(E - E_i)}} \qquad \text{(XII)}$$

where

$$\tilde{B} = \frac{h^2}{2\mu(\Delta q)^2} \qquad \text{(XIII)}$$

It can be noted here that formula XII coincides with the expression for the energy dependence of the density of states function of a free one-dimensional rotor with the rotational constant equal to $\tilde{B}$. It is convenient to use this equivalence of formulas in practical calculations where computer subroutines written for one-dimensional rotors can be used to treat the degree of freedom associated with the motion along the PES ridge.

The transition state sum-of-states function is then given by

$$W^{\neq}(E) = \sum_i \int_0^E \frac{d\epsilon\, W_{2,i}(E-\epsilon)}{\sqrt{\tilde{B}_i(\epsilon - E_i)}} = \sum_i \int_0^{E-E_i} \frac{dx\, W_{2,i}(E-x-E_i)}{\sqrt{\tilde{B}x}} = \sum_i \tilde{W}_i^{\neq}(E-E_i) \qquad \text{(XIV)}$$

(a variable substitution $x = \epsilon - E_i$ was used here). The $\tilde{W}_i^{\neq}(E - E_i)$ functions have the meaning of sum-of-states functions of pseudo-transition states corresponding to the individual segments. These pseudo-transition states are positioned at energies E_i and have $N - 1$ degrees of freedom. Of these, $N - 2$ are the "ordinary" degrees of freedom orthogonal to the motion along the PES ridge (q coordinate). The last degree of freedom associated with the q coordinate is substituted here by a pseudo-rotation with the rotational constant given by expression XIII. Thus, the energy-dependent rate constant can be represented as

$$k(E) = \sum_i \tilde{k}_i(E) \qquad \text{(XV)}$$

where $\tilde{k}_i(E)$ are energy-specific rate constants computed using the above pseudo-transition states.

II.2. General Case of Thermally Averaged Rate Constants of a Bimolecular or Unimolecular Reaction. The partition function of a transition state, in the classical limit, is given by

$$Q_{CL}^{\neq}(\beta) = \frac{1}{h^{N-1}} \int d\mathbf{p}\, d\mathbf{q}\, \exp(-\beta H(\mathbf{p},\mathbf{q})) \qquad \text{(XVI)}$$

where $\mathbf{p}$ and $\mathbf{q}$ are the $(N - 1)$-dimensional momentum and coordinate, $H(\mathbf{p},\mathbf{q})$ is the transition state Hamiltonian, $\beta = (k_B T)^{-1}$ is an inverse reduced temperature, and h is the Planck constant. Provided that the motion along the PES ridge (coordinate q_1 and momentum p_1) can be locally separated from the remaining $N - 2$ degrees of freedom of the transition state, i.e., the Hamiltonian can be represented as

$$H(\mathbf{p},\mathbf{q}) = H_{N-2}(\mathbf{p}_{N-2},\mathbf{q}) + \frac{p_1^2}{2\mu} + V(q_1) \qquad \text{(XVII)}$$

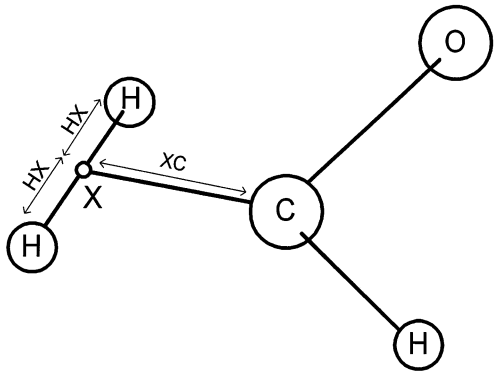

Figure 3. The system of coordinates designed to facilitate the description of the H_2-eliminating channel. A "dummy" atom (X) is positioned in the middle of the segment connecting the two H atoms that are expected to form H_2 in reaction channel 3b. The variables HX and XC are scanned (the rest of the variables are optimized) to obtain the PES shown in Figures 4−8. The details of the Z-matrix used are given in the Supporting Information.

we can take the integral in XVI over the $N - 2$ degrees of freedom and p_1 thus obtaining

$$Q_{CL}^{\neq}(\beta) = \sqrt{\frac{2\pi\mu}{h^2\beta}} \int dq_1\; Q_{N-2}^{\neq}(\beta,q_1) \exp(-\beta V(q_1)) \qquad \text{(XVIII)}$$

Here, $Q_{N-2}^{\neq}(\beta,q_1)$ is a partition function of the $N - 2$ degrees of freedom (motion along the PES ridge excluded) which, generally, can depend on q_1. Note that in expression XVII the Hamiltonian of the $N - 2$ degrees of freedom, $H_{N-2}(\mathbf{p}_{N-2},\mathbf{q})$, can depend on q_1.

Substituting the integral in XVIII with summation over the pseudo-transition states indexed by i in a way similar to that used in subsection II.1, we obtain

$$Q_{CL}^{\neq}(\beta) = \sum_i \tilde{Q}_i^{\neq}(\beta) \qquad \text{(XIX)}$$

and, through the transition state theory formula[40] for the rate constant ($k(T)$),

$$k(T) = \sum_i \tilde{k}_i(T) \qquad \text{(XX)}$$

Here, $\tilde{Q}_i^{\neq}(\beta)$ is the partition function of the ith pseudo-transition state with $N - 2$ "ordinary" degrees of freedom and one extra pseudorotation with the effective rotational constant given by expression XIII. $\tilde{k}_i(T)$ are the rate constants calculated for the individual pseudo-transition states using $\tilde{Q}_i^{\neq}(\beta)$ and the transition state theory formula.[40] For unimolecular reactions in the high-pressure limit, expression XX coincides with what would be obtained by averaging expression XV over the Boltzmann energy distribution.

III. Potential Energy Surface of the O + CH_3 System

The study of the potential energy surface (PES) of the O + CH_3 system was performed with an emphasis placed on the routes of decomposition of the CH_3O adduct formed in the initial reaction act. A relaxed scan of the PES was performed using four methods: UHF, UMP2, QCISD, and density functional B3LYP method with the 6-311G(d,p) basis set (ref 41 can be consulted for details of the methods and the basis set). The system of coordinates (designed to facilitate the description of the H_2-eliminating channel) employed in the study is illustrated in Figure 3. A "dummy" atom (X) was positioned in the middle

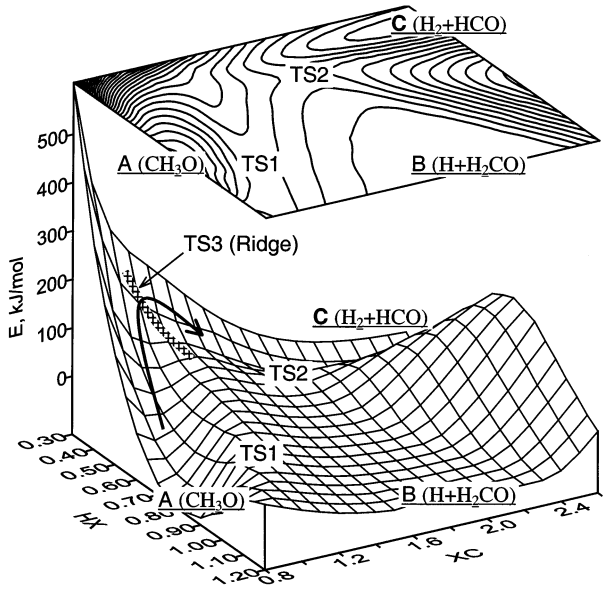

Figure 4. 3-dimensional surface and contour plots (energy as a function of HX and XC) of the PES obtained at the UMP2/6-311G(d,p) level. Valleys A, B, and C represent the CH_3O adduct, H + H_2CO, and H_2 + HCO, respectively. Saddle point TS1 is the transition state for the decomposition of CH_3O to H + H_2CO (reaction 3a); TS2 is the transition state for the abstraction reaction H + $H_2CO \rightarrow H_2$ + HCO. There is no saddle point corresponding to the transition state of the $CH_3O \rightarrow H_2$ + HCO (3b) reaction. However, the PES ridges between the A and B valleys and between the B and C valleys converge at low values of HX and XC and form a single ridge that separates the valleys A (CH_3O) and C (H_2 + HCO). The wide crosshatched line marked as TS3 represents the approximate location of this PES ridge. Trajectories originating in the reactant valley (A) and crossing this ridge are likely to proceed to the H_2 + HCO products (as indicated by the curved arrow), thus representing reaction 3b.

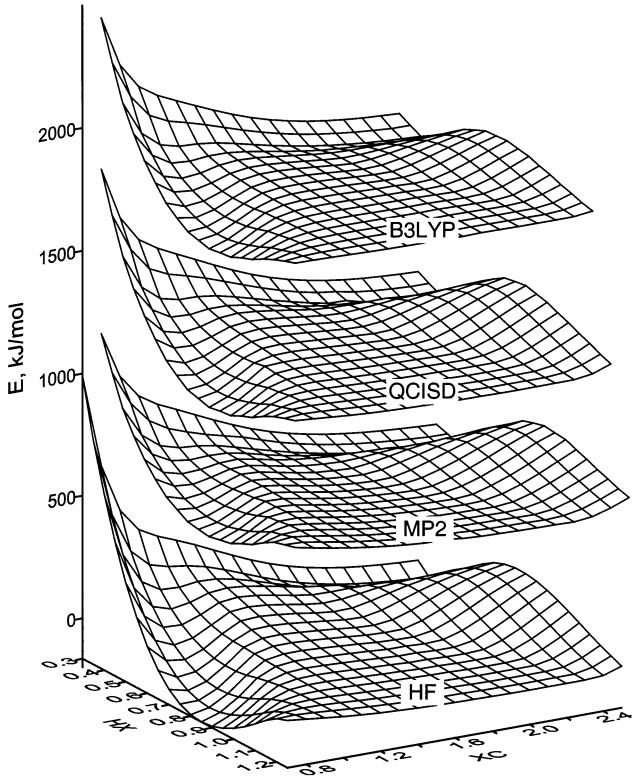

Figure 5. Three-dimensional surface plots (energy as a function of HX and XC) of the PES obtained in calculations using the UHF, UMP2, QCISD, and B3LYP methods with the 6-311G(d,p) basis set. Surfaces obtained with different methods are shifted relative to each other along the energy axis to avoid overlapping. The figure serves to demonstrate that similar shapes of PES were obtained at all levels of calculation. The qualitative character of PES (i.e., the existence of the TS1 and TS2 saddle points and the TS3 region responsible for the $CH_3O \rightarrow H_2$ + HCO reaction) appears to be independent of the computational method used.

of the segment connecting the two H atoms that are expected to form H_2 in reaction channel 3b. Two variables, HX (half the H−H distance) and XC (the distance between the C atom and X), were fixed at a series of equidistant periodic values while the rest of the variables were optimized. The details of the Z-matrix used are given in the Supplement. The Gaussian 98 system of programs[42,43] was used in all quantum chemistry calculations.

III.1. Qualitative Shapes of PES. The results of PES scans performed using the above four methods, despite the different values of energy barriers, yielded similar results in terms of the qualitative description of the major PES properties. Figure 4 presents a three-dimensional surface and contour plots (energy as a function of HX and XC) of the PES obtained at the UMP2/6-311G(d,p) level. Valleys A, B, and C represent the CH_3O adduct, H + H_2CO, and H_2 + HCO, respectively. The saddle point TS1 is the transition state for the decomposition of CH_3O to H + H_2CO (reaction 3a); TS2 is the transition state for the abstraction reaction H + $H_2CO \rightarrow H_2$ + HCO. There is no saddle point corresponding to the transition state of reaction 3b, i.e., the transformation leading from the CH_3O adduct to the H_2 + HCO products. However, as can be seen from Figure 4, the PES ridges between the A (CH_3O) and B (H+H_2CO) valleys and between the B (H + H_2CO) and C (H_2 + HCO) valleys converge at low values of HX and XC and form a single ridge that separates the valleys A (CH_3O) and C (H_2 + HCO). The wide crosshatched line marked as TS3 represents the approximate location of this PES ridge. Trajectories originating in the reactant valley (A) and crossing this ridge are likely to proceed to the H_2 + HCO products, thus representing reaction channel 3b. As can be seen from Figure 5, similar shapes of the PES were obtained at the HF, MP2, QCISD, and B3LYP levels of calculation. The qualitative character of the PES (i.e., the existence of the TS1 and TS2 saddle points and the TS3 region responsible for the $CH_3O \rightarrow H_2$ + HCO reaction) appears to be independent of the computational method used.

The qualitative shape of the PES of reaction 1 obtained in the current study is somewhat similar to that of the PES for the system of the CN + $H_2 \rightarrow$ H + HCN and the $H_2CN \rightarrow$ H + HCN reactions reported by ter Horst et al.[44] The latter is characterized by the existence of a PES ridge separating the H_2CN valley and the CN + $H_2 \rightarrow$ H + HCN reaction path and by the absence of a saddle point leading from H_2CN to the CN + H_2 products.

III.2. Dividing Surface. The hypothesis that the TS3 region of the PES represents the dividing surface between the A and the C valleys was verified by performing IRC (intrinsic reaction coordinate or steepest descent path)[34] calculations in mass-weighted internal coordinates[45] using locations in the vicinity of TS3 as starting points (Figure 6). For the calculation of the rate constants, one needs to specify the location of the dividing line, or the ridge separating the A valley (reactant) from the B and the C valleys (products). The terms "dividing line" and "ridge" will be used interchangeably henceforth. Also, one needs to identify the "critical point" on that dividing line such that the trajectories passing over the ridge to the left (in Figures 4−7) of this point proceed to valley C (H_2 + HCO) and those passing on the right of this point−to valley B (H + H_2CO).

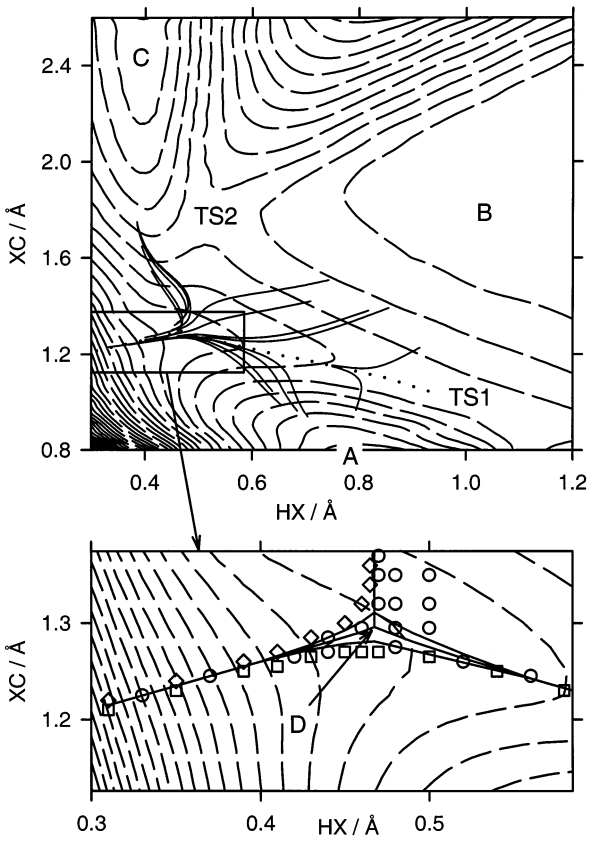

Figure 6. Contour plots of the potential energy surface (PES, energy as a function of HX and XC) of reaction 3 obtained at the UMP2/6-311G(d,p) level of calculations. Nomenclature of the valleys and saddle points is the same as in Figure 4. Dashed lines: lines of equal energy levels (step sizes 20 kJ mol^{-1} in the upper graph and 10 kJ mol^{-1} in the lower graph). Upper graph: low resolution PES map. Solid curved lines show examples of IRC (intrinsic reaction coordinate or steepest descent path)[34] trajectories calculated in mass-weighted internal coordinates[45] using locations in the vicinity of the PES ridge separating valleys A and C (or B) as starting points. The dotted line represents the location of the PES ridge. Lower graph: higher resolution map of the area of the PES ridge indicated by rectangle in the upper plot. A representative selection of IRC starting points is displayed by symbols. Different symbols represent the PES valley to which the corresponding IRC trajectory descends: squares, valley A (CH_3O); circles, valley B ($H + CH_2O$); diamonds, valley C ($H_2 + HCO$). Solid lines indicate the location of the three PES ridges (1−3, see text) intersecting in point D. The dividing line running from left to right (formed by ridges 1 and 3) is indicated by three lines coinciding at the edges of the graph but deviating from each other near the intersection point D: central, upper, and lower lines. The upper and the lower lines correspond to the alternative "upper" and "lower" dividing lines (section III) which encompass the area of uncertainty of the location of point of intersection of the ridges. Ridge 1 located to the right of point D is responsible for the $CH_3O \rightarrow H + CH_2O$ reaction channel and ridge 3 located to the left of point D is responsible for the $CH_3O \rightarrow H_2 + HCO$ reaction.

Identification of such a critical point is not unambiguous. To the best of the author's knowledge, no rigorous mathematical procedures have yet been developed for this purpose. The procedure used here is described below and the uncertainties associated with the selection of the critical point are discussed in sections V and VI.

It can be noted that the two PES ridges, (1) separating the A and the B valleys and (2) separating the B and the C valleys converge (at approximately HX = 0.45 and XC = 1.25 on the UMP2-level PES, Figure 6) and form the third ridge (3) separating the A and the C valleys. Ridges 1 and 3 form the "dividing line" mentioned above. It seems natural to identify the critical point on the dividing line with the point of intersection of the three ridges. This approach was, therefore, adopted in the current study. As will be shown below, a certain degree of uncertainty is associated with determining the exact location of the point of intersection. The actual implementation of the search for this point uses linearization of the PES ridges in the (HX, XC) coordinate plane.

The method used to locate this point of intersection is based on the analysis of the IRC paths. IRC calculations were performed in the "downhill" mode (i.e., the first step is performed in the direction of the PES gradient) using starting points in the vicinities of the expected locations of ridges 1, 2, and 3. The stabilities of calculated IRC paths relative to the details of computational procedures used were confirmed by comparing the results obtained with different step sizes (0.01−0.04 amu$^{-1/2}$ Bohr), different convergence criteria, and different methods of obtaining the force constants for steps other than the first one ("CalcAll" vs "CalcFC" options of Gaussian[42]).

IRCs started in the vicinity of a PES ridge tend to run along the ridge before deviating to one of its sides.[3] This does not complicate the analysis when the downhill motion along the ridge leads to a saddle point since the IRC trajectories will converge to one or the other side of the ridge when they approach the saddle point. However, when the ridge separates into two, the situation is different. In the current study, it was observed that while some of the IRCs started in the vicinity of PES ridge 3 propagated into valley A (CH_3O) and others into valley C ($H_2 + HCO$), there was a fraction of IRCs that ran along the PES ridge and, after passing the point of intersection of the ridges, descended between ridges 1 and 2 into valley B ($H + H_2CO$). In the upper part of ridge 3 (at HX = 0.3−0.4 Å), the area from which IRCs descended to valley B was a narrow (less than 0.01 Å width in the XC direction) line running along the ridge. However, this "valley B IRCs" area widened near the intersection of the ridges, thus complicating the identification of the point of intersection. This is illustrated in Figures 6 and 7 where selected IRCs starting points are shown with different symbols indicating the valley to which these IRCs descended.

In the PES areas outside the immediate vicinity of the intersection of the ridges the locations of the ridges could be identified with relatively high accuracy, 0.005−0.01 Å. The point of intersection and the ridges in its vicinity could only be approximately located by extrapolating the directions of the ridges from the "certain" areas into the "uncertain" one. The thus determined PES ridges are indicated in Figures 6 and 7 (lower graphs) by solid lines. The line passing from the left to the right along ridges 3 and 1 represents the "dividing line" which separates the reactants from the products. At the same time, for the purpose of estimating the uncertainties, alternative "upper" and "lower" dividing lines were drawn in the HX−XC coordinate plane passing over the area of uncertainty at higher and lower values of XC, respectively (upper and lower solid lines in the lower graphs of Figures 6 and 7). Effects of using these alternative dividing lines on channel branching were investigated (section IV). Similarly, effects of variation in the location of the critical (intersection) point along the dividing line were evaluated, as described in section IV.

This analysis was performed using the PES obtained at the UMP2/6-311G(d,p) and density functional B3LYP/6-311G(d,p) levels. The resultant dividing line was taken as representing the PES ridge separating the reactant and the product valleys. To obtain a more accurate evaluation of the potential energy profile along the PES ridge, single-point G2[46] and CBS-Q[47] calculations

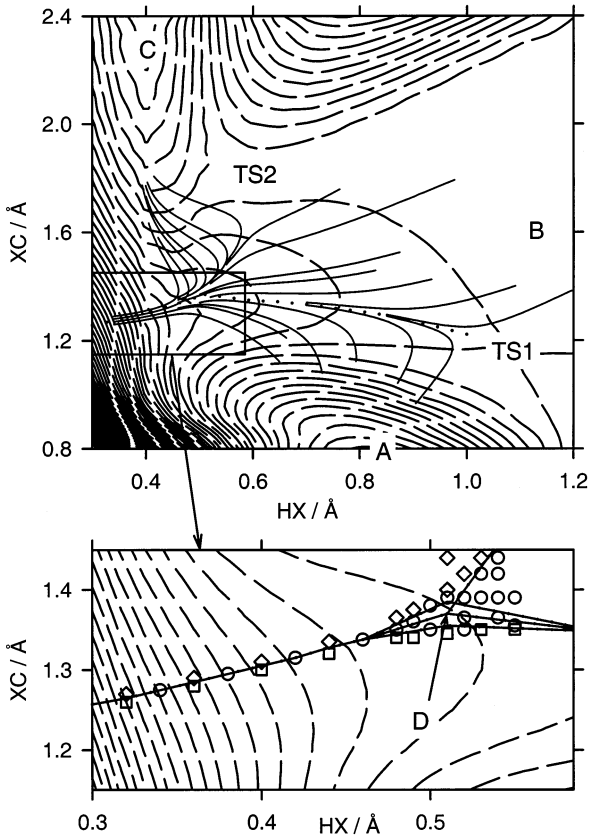

Figure 7. Same as Figure 6 but with the PES obtained at the B3LYP/6-311G(d,p) level.

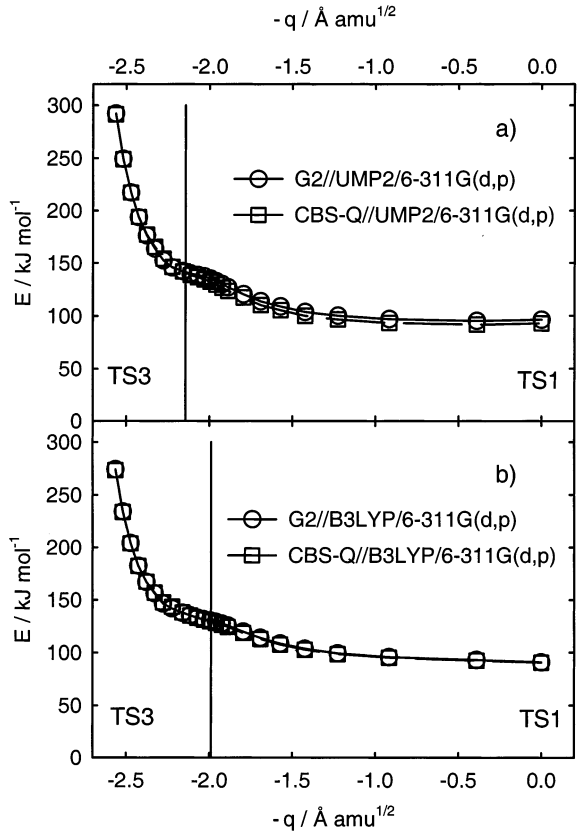

Figure 8. (a) Energy values calculated using the G2[46] (circles and solid line) and CBS-Q[47] (squares and dashed line) methods at selected points along the dividing line (PES ridge) on the UMP2 surface. Energy values include the zero-point vibrational energy and are given relative to CH_3O. The vertical solid line marks the position of the critical point (point D in Figures 6 and 7). The part of the PES ridge to the left of the vertical line ($q > 2.14$ Å amu$^{1/2}$) represents the dividing surface (TS3) for reaction 3b ($CH_3O \rightarrow H_2 + HCO$) and that to the right of the vertical line ($q < 2.14$ Å amu$^{1/2}$) corresponds to the dividing surface (TS1) for reaction 3a ($CH_3O \rightarrow H + H_2CO$). The negative direction for the q variable is chosen to conform to the orientation of the dividing line in Figures 6 and 7. (b) The same as in part (a) but for the B3LYP-level potential energy surface. The vertical line is positioned at $q =$ 1.99 Å amu$^{1/2}$.

were performed for a sequence of configurations along the dividing line and for the CH_3O equilibrium configuration. The resultant potential energy profiles along the dividing line are shown in Figure 8. As can be seen from the plots, the G2 and the CBS-Q level profiles differ very little (less than 3.6 and 1.6 kJ mol^{-1} with the UMP2- and the B3LYP-level surfaces, respectively).

The values of the coordinate q associated with the motion along the dividing line (PES ridge) were assigned by consecutive addition of the increments of q between a sequence of points selected on the line. The values of these increments (δq) were obtained from the corresponding increments of the mass-weighted Cartesian coordinates in the coordinate system defined by the principal axes of inertia:

$$(\delta q)^2 = \sum_j \sum_{n=1}^{3} m_j (\delta x_{j,n})^2 \qquad \text{(XXI)}$$

where indices j and n indicate atoms and their Cartesian coordinates, respectively. The Hamiltonian of the degree of freedom corresponding to the motion along the dividing PES ridge is thus reduced to that of a unit mass in the $V(q)$ potential (Figure 8). The values of q and $V(q)$ at the selected points along the dividing line are presented in Table 1.

Calculation of the energy-dependent rate constants $k(E)$ of the channel of decomposition of CH_3O to $H_2 + HCO$ (channel 3b) requires knowledge of the properties of the degrees of freedom of the reactive system on the dividing surface other than the degree of freedom associated with the motion along the dividing line. Projected[33,48] vibrational frequencies were calculated for the same sequence of points on the dividing line as was used in the $V(q)$ calculation above (Table 1). Calculations were performed using both the UMP2 and the B3LYP method. The resultant values of the projected frequencies and their approximate assignment are listed in Table 2. As can be seen from the table, in the majority of the points, one of the frequencies is imaginary and the rest are real. The imaginary frequency was associated with the system's motion across the ridge, i.e., the reaction coordinate. In the part of the dividing line corresponding to low HX values, two or even three frequencies instead of one were imaginary. Visualized normal modes associated with the second and the third imaginary frequencies can be described as hindered incomplete rotations of the H−X−H fragment: the second mode is similar to torsion about the X−C axis and the third one to rocking in the plane formed by the H−X−H and the X−C lines. These "faulty" second and third imaginary frequencies appear in the area of the PES with a large gradient in the direction of lower HX. If the PES is scanned using linear increments in the directions of the vectors of these "faulty" normal modes, the HX variable (and thus the H−H distance) increases during the scan, which results in a decrease of energy and explains the negative second derivatives of energy.

For the purpose of calculation of the rate constants, the second derivatives of these "faulty" modes were estimated by performing relaxed PES scans using partial H−X−H rotations (preserv-

TABLE 1: Selected Points along the PES Ridge (Dividing Line)

point number[a]	HX/Å	XC/Å	q/Å amu$^{1/2}$ [b]	E(G2)[c]/ h	E(CBS-Q)[c]/h	ZPVE [d]/kJ mol^{-1}	E(G2) + ZPVE[e]/kJ mol^{-1}	E(CBS-Q) + ZPVE[e]/kJ mol^{-1}
				UMP2 Surface				
M1	0.3	1.210	2.564	−114.781 401	−114.787 223	70.75	195.95	198.51
M2	0.32	1.220	2.519	−114.797 476	−114.803 165	70.11	153.11	156.02
M3	0.34	1.230	2.472	−114.809 470	−114.815 024	69.48	120.98	124.24
M4	0.36	1.240	2.425	−114.818 337	−114.823 739	69.02	97.25	100.91
M5	0.38	1.250	2.377	−114.824 811	−114.830 000	68.64	79.87	84.09
M6	0.4	1.260	2.328	−114.829 463	−114.834 359	68.25	67.27	72.25
M7	0.42	1.270	2.278	−114.832 744	−114.837 708	65.80	56.20	61.01
M8	0.44	1.280	2.223	−114.835 021	−114.840 356	64.97	49.39	53.23
M9	0.46	1.291	2.161	−114.836 581	−114.842 232	65.63	45.96	48.96
M10[f]	0.4675	1.296	2.1448	−114.837 033	−114.842 786	65.63	44.76	47.50
M11	0.48	1.287	2.114	−114.837 684	−114.843 757	66.20	43.63	45.53
M12	0.5	1.275	2.071	−114.838 790	−114.845 178	67.76	42.28	43.35
M13	0.52	1.264	2.031	−114.839 956	−114.846 525	69.43	40.89	41.49
M14	0.54	1.253	1.994	−114.841 155	−114.847 832	70.59	38.90	39.21
M15	0.56	1.243	1.959	−114.842 385	−114.849 140	71.30	36.39	36.50
M16	0.58	1.233	1.924	−114.843 614	−114.850 416	71.74	33.60	33.59
M17	0.6	1.223	1.888	−114.844 846	−114.851 683	72.04	30.67	30.56
M18	0.65	1.198	1.795	−114.847 547	−114.854 234	72.46	24.00	24.28
M19	0.7	1.178	1.692	−114.850 113	−114.856 995	72.68	17.47	17.25
M20	0.75	1.158	1.572	−114.851 990	−114.858 852	72.67	12.54	12.36
M21	0.8	1.128	1.424	−114.854 093	−114.860 979	73.00	7.34	7.11
M22	0.85	1.103	1.225	−114.855 367	−114.862 248	72.89	3.89	3.67
M23	0.9	1.068	0.916	−114.856 713	−114.863 608	73.22	0.69	0.43
M24	0.95	1.033	0.39	−114.857 355	−114.864 193	73.16	−1.06	−1.17
M25[g]	0.980	1.011	0	−114.857 399	−114.864 195	74.33	0.00	0.00
M26[h]	*0.886*	*0.651*		*−114.903 583*	*−114.909 122*	*99.31*	*−96.28*	*−92.98*
				B3LYP Surface				
D1	0.32	1.265	2.542	−114.802 565	−114.808 328	65.42	234.31	233.69
D2	0.34	1.275	2.496	−114.813 811	−114.819 478	64.81	204.18	203.81
D3	0.36	1.285	2.447	−114.821 967	−114.827 533	64.45	182.41	182.31
D4	0.38	1.295	2.396	−114.827 792	−114.833 237	64.36	167.03	167.24
D5	0.4	1.305	2.343	−114.831 880	−114.837 179	64.30	156.23	156.83
D6	0.42	1.315	2.287	−114.834 713	−114.839 830	61.95	146.44	147.52
D7	0.44	1.3275	2.223	−114.836 748	−114.841 683	62.71	141.86	143.41
D8	0.46	1.3375	2.162	−114.838 138	−114.843 513	62.13	137.63	138.03
D9	0.48	1.3505	2.093	−114.839 277	−114.844 865	62.74	135.24	135.08
D10	0.5	1.3635	2.023	−114.840 290	−114.845 884	63.17	133.01	132.84
D11[f]	0.51	1.37	1.989	−114.840 794	−114.846 327	63.36	131.88	131.87
D12	0.52	1.3675	1.969	−114.841 165	−114.846 824	63.85	131.40	131.05
D13	0.54	1.3625	1.932	−114.841 980	−114.847 817	64.95	130.37	129.55
D14	0.56	1.3575	1.897	−114.842 873	−114.848 824	66.06	129.12	128.01
D15	0.58	1.3525	1.863	−114.843 823	−114.849 845	66.95	127.52	126.22
D16	0.6	1.3475	1.830	−114.844 804	−114.850 876	67.63	125.63	124.20
D17	0.65	1.3425	1.744	−114.847 361	−114.853 371	68.53	119.81	118.54
D18	0.7	1.3325	1.656	−114.849 756	−114.855 707	68.99	113.98	112.87
D19	0.75	1.3225	1.556	−114.851 953	−114.857 852	69.21	108.44	107.46
D20	0.8	1.3075	1.438	−114.853 859	−114.859 718	69.32	103.54	102.67
D21	0.85	1.2925	1.297	−114.855 526	−114.861 320	69.40	99.24	98.54
D22	0.9	1.2725	1.121	−114.856 893	−114.862 646	69.45	95.70	95.11
D23	0.95	1.2475	0.894	−114.857 960	−114.863 693	69.47	92.93	92.39
D24	1	1.2225	0.609	−114.858 787	−114.864 467	69.48	90.76	90.36
D25[g]	1.083	1.1599	0.000	−114.859 333	−114.865 002	70.80	90.65	90.27
D26[h]	*0.8836*	*0.6639*		*−114.903 487*	*−114.909 014*	*96.08*	*0.0*	*0.0*

[a] The same numbering is used in Tables 1−3. [b] 1 amu = 1.6606 × 10^{-27} kg. [c] Single-point energy calculations performed using the G2[46] and CBS-Q[47] methods. Energy values are in units of hartree (1 h = 2625.5 kJ mol^{-1}). [d] Zero-point vibrational energy (computed from the values of vibrational frequencies in Table 2). [e] Energies relative to the transition state TS1 (transition state for reaction 3a, $CH_3O \rightarrow H + H_2CO$) for the UMP2 surface and relative to the CH_3O equilibrium configuration for the B3LYP surface. [f] Critical point on the dividing line. [g] Transition state TS1. [h] Equilibrium configuration of CH_3O. Italics are used to emphasize that this point is not on the PES ridge.

ing the H−H distance) instead of linear normal mode vectors. Scans of the HXCO dihedral angle and of the HXC angle were used for the "torsional" and the "rocking" degrees of freedom, respectively. These second derivatives of energy resulted in the values of the corresponding vibrational frequencies given in Table 2. To verify the adequacy of this procedure, frequencies estimated via such scans were compared with the values obtained in the Gaussian 98 projected frequencies analysis at large H−H separations, where the above influence of the PES gradient can be expected to be unimportant. At HX = 0.50 and HX = 0.70 Å, the differences between the vibrational frequencies obtained via these two different methods did not exceed 15% (Table 2). An attempt to evaluate the potential effects of uncertainties in the frequencies of these "faulty" modes was made by performing rate constant calculations with the values of these frequencies doubled or reduced by half (see section IV).

The transition state for reaction channel 3a ($CH_3O \rightarrow H + H_2CO$) is symmetric with the departing H, C, and O atoms positioned in the plane of symmetry. The departing H atom (H1)

TABLE 2: Projected Frequencies Obtained at Selected Points along the PES Ridge

	modes[a]							
point number[b]	1[c]	2[d]	3[e]	4[f]	5[g]	6[h]	7[i]	8[j]
			UMP2 Surface					
M1	421i	1075[k] (2992i)	2017[k] (2251i)	856	1302	1629	1844	3106
M2	621i	1069[k] (2402i)	1911[k] (1602i)	882	1281	1628	1837	3113
M3	1094i	1059[k] (1885i)	1782[k] (667i)	910	1268	1640	1837	3119
M4	1034i	1047[k] (1424i)	1652[k] (293)	942	1267	1666	1842	3124
M5	1186i	1027[k] (906i)	1517[k] (704)	975	1278	1699	1854	3127
M6	1244i	1005[k] (385i)	1381[k] (840)	1001	1291	1730	1876	3126
M7	1296i	978[k] (541i)	921	1020	1300	1749	1909	3122
M8	1311i	713	1040	992	1301	1753	1951	3113
M9	1257i	750	1040	1061	1290	1734	2001	3098
M10[l]	1198i	739	1052	1066	1282	1719	2024	3089
M11	1301i	759	1048	1074	1310	1760	2026	3091
M12	1351i	783[890][m]	1040[963][m]	1113	1375	2048	1879	3089
M13	1378i	789	1046	1145	1429	2159	1955	3084
M14	1423i	782	1057	1169	1459	2296	1962	3077
M15	1470i	769	1069	1187	1478	2396	1954	3069
M16	1510i	754	1078	1201	1491	2469	1941	3061
M17	1542i	740	1086	1214	1501	2526	1924	3053
M18	1593i	711	1099	1239	1521	2634	1874	3036
M19	1598i	662[566][m]	1096	1257	1537	2730	1850	3018
M21	1602i	623	1090	1281	1559	2857	1795	3001
M22	1564i	599	1077	1287	1565	2875	1790	2992
M23	1570i	603	1096	1291	1567	2920	1770	2995
M24	1450i	591	1119	1293	1567	2913	1765	2984
M25[n]	1579i	572	1289	1294	1570	2934	1770	2997
			B3LYP Surface					
D1	353i	1018[k] (2378i)	1658[k] (1818i)	850	1471	1216	1723	3002
D2	502i	1002[k] (1861i)	1545[k] (1297i)	870	1487	1208	1713	3009
D3	1398i	990[k] (949i)	1444[k] (383i)	892	1211	1516	1707	3015
D4	1012i	973[k] (879i)	1368[k] (492)	916	1221	1558	1704	3020
D5	1016i	951[k] (449i)	1291[k] (720)	940	1236	1606	1703	3023
D6	1066i	926[k] (436)	837	959	1254	1653	1706	3023
D7	1087i	892[k] (611)	918	978	1272	1715	1691	3018
D8	1108i	660	946	1015	1295	1745	1713	3013
D9	1100i	661	945	1054	1318	1782	1725	3004
D10	1076i	640	934	1083	1342	1832	1736	2994
D11[l]	1056i	624	927	1095	1354	1741	1861	2989
D12	1045i	618	924	1105	1370	1926	1741	2990
D13	989i	607	929	1123	1398	2072	1741	2990
D14	926i	594	941	1140	1419	2221	1740	2989
D15	880i	581	953	1153	1435	2345	1738	2987
D16	848i	568	963	1165	1448	2441	1736	2985
D17	793i	526	977	1188	1469	2587	1736	2975
D18	763i	496	981	1205	1483	2671	1733	2965
D19	734i	468	978	1219	1493	2726	1731	2955
D20	715i	448	973	1230	1501	2764	1727	2945
D21	690i	426	966	1239	1508	2801	1727	2936
D22	670i	411	959	1246	1513	2829	1726	2927
D23	656i	400	953	1251	1516	2850	1724	2922
D24	633i	386	947	1254	1518	2867	1724	2919
D25[n]	649i	378	1163	1257	1521	2873	1723	2920

[a] Assignment of normal modes is not easily performed on the PES ridge as atom displacements do not conform to traditional types (stretch, rock, etc.). The mode assignment given here is that of the transition state TS1 for the $CH_3O \rightarrow H + CH_2O$ reaction, configurations M25 and D25 in the Table. [b] Numbering of points corresponds to that used in Table 1. [c] Reaction coordinate, motion across the ridge. Departing H stretch in the transition state TS1. [d] O−C···H bend (At low HX, this mode can be described as H−X−H torsion about the X−*C* axis.). [e] CH_2 wag (At low HX, this mode can be described as H−X−H rocking in the plane formed by the H−X−H and the X−C lines.). [f] CH_3 rock. [g] H−C−H bend. [h] C−H stretch. [i] C−O stretch. [j] C−H stretch (H atom remaining as part of HCO or H_2CO). [k] Frequency values were estimated from PES scans. Original values of projected frequencies affected by the large PES gradient in the direction of increasing HX (see text, section III) are provided in parentheses. [l] Critical point on the dividing line. [m] Frequency values estimated from PES scans are given in square brackets (see text, section III). [n] Transition state (TS1) for reaction 3a. One additional vibrational mode corresponding to a H−C···H bend (motion along the PES ridge) has frequencies of 608 cm^{-1} (UMP2 PES) or 412 cm^{-1} (B3LYP PES).

is equidistant from the two remaining H atoms of CH_3O (H2 and H3, the numbers are assigned here for the clarity of description). If one moves from this configuration along the PES ridge 1 toward the point of intersection of the ridges, the symmetric structure becomes distorted and the distance between the departing H atom (H1) and one of the remaining H atoms (H2) becomes smaller. In the area past the point of ridge intersection, atoms H1 and H2 are very close and form the H2 molecule that departs from the remaining HCO fragment; this part of the PES corresponds to ridge 3, the "transition state" for the reaction channel 3b. A similar distortion of the symmetric structure obtained by moving along the PES ridge in the other direction, such that the H1 atom becomes closer to H3 (instead of H2), will result in an equivalent potential energy profile and in a system of PES ridges symmetric to the one considered above relative to the H2 ↔ H3 substitution. These two systems

related by the H2 ↔ H3 substitution cannot be transformed one into another by rotations and thus are optical isomers (Here, the meaning of the term "optical isomers" is the same as the one used in refs 9, 49, and 50 in relation to reaction path degeneracy, i.e., mirror images that are not superimposable.). Therefore, points along the PES ridge listed in Tables 1 and 2 have their equivalent counterparts at negative values of the q coordinate where $V(-q) = V(q)$. In Figure 8, the range of q from zero to the vertical line indicating the position of the critical point represents only a half of the range of q corresponding to the transition state for the reaction channel 3a. Similarly, the area to the left of the vertical line (Figure 8) responsible for the reaction channel 3b has an equivalent counterpart at negative values of q.

IV. Energy-Dependent Rate Constants *k(E)* and Branching Fractions for Channels 1a and 1c.

IV.1. Procedure and Results. For the purpose of calculation of the energy-specific rate constants $k(E)$, the q coordinate of the motion along the dividing line was subdivided into 24 segments: 15 segments (14 for the B3LYP surface) of varying widths were used for the part of the dividing line corresponding to the $CH_3O \rightarrow H + H_2CO$ (channel 3a) reaction and another nine segments (10 for the B3LYP surface) for the part corresponding to the $CH_3O \rightarrow H_2 + HCO$ (channel 3b) reaction. Each segment was centered on one of the PES points listed in Tables 1 and 2. The border between the segments located on the two sides of the critical point was slightly adjusted to coincide with the coordinate of the critical point. Only half of the segment associated with the transition state TS1 was used. Each segment was assigned vibrational frequencies and G2 or CBS-Q-level energy values of the associated PES point in Tables 1 and 2. The dividing surface (or "transition state") was thus subdivided into 24 pseudo-molecules (or pseudo-transition states) with 7 vibrational degrees of freedom and one pseudorotation (rotational constant given by formula XIII) positioned at energies E_i, as described in section II. Energies, rotational constants, and vibrational frequency assignments of individual pseudo-molecules are presented in Table 3.

The energy-specific rate constants $\tilde{k}_i(E)$ for each pseudo-transition state were calculated using formulas XII−XIV of section II. The overall $k(E)$ dependences for channels 3a and 3b were obtained by summation over i (e.g., $i = 1-15$ for channel 3a and $i = 16-24$ for channel 3b using the UMP2 PES). One one-dimensional overall rotational degree of freedom was treated as active[9−12] in all transition states and the CH_3O molecule. A reaction degeneracy factor of 3 was used for reactions 3a and 3b, as results from the symmetry factor of 3 in the CH_3O molecule (see refs 9, 49, and 50). The values of $k_{3a}(E)$ and $k_{3b}(E)$ calculated by summation of the $\tilde{k}_i(E)$ dependences for appropriate i ranges were multiplied by two to account for the fact that segments 1−24 represent only half of the range of q coordinate corresponding to the transition states for reactions 3a and 3b (the other half of the $V(q)$ potential corresponds to negative q, $V(q) = V(-q)$, see above, section III).

$k(E)$ calculations were performed using four models: those resulting from the G2 and CBS-Q potential energy profiles along the dividing lines obtained on the UMP2 and B3LYP potential energy surfaces. The resultant $k_{3a}(E)$ and $k_{3b}(E)$ dependences are presented in Figures 9 and 10. Also shown in Figures 9 and 10 are the dependences on energy of the energy-specific branching ratio of channels 3b and 3a, $\gamma(E) = k_{3b}(E)/k_{3a}(E)$. As can be seen from the plots, $\gamma(E)$ increases with energy,

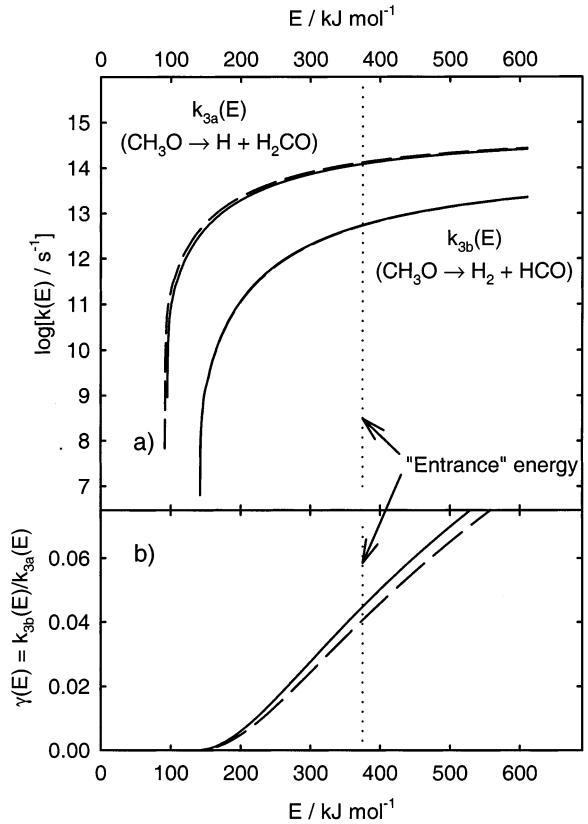

Figure 9. (a) Energy dependences of the microscopic $k(E)$ rates of reaction channels 3a and 3b obtained using the UMP2/6-311G(d,p) potential energy surface with G2[46] (solid lines) and CBS-Q[47] (dashed lines) energies calculated along the dividing line (PES ridge). The solid and the dashed lines are indistinguishable for the $k_{3b}(E)$ dependence. (b) Energy dependence of the energy-specific branching ratio of channels 3b and 3a, $\gamma(E) = k_{3b}(E)/k_{3a}(E)$. The dotted vertical line on both plots marks the energy of the "entrance" channel of the chemically activated $O + CH_3 \rightarrow CH_3O^* \rightarrow$ products (1) reaction.

reaching the values of 0.045 (0.041) and 0.074 (0.073) (obtained with the G2 (CBS-Q) energy profiles along the dividing line obtained on the UMP2 and B3LYP PES, respectively) at the energy of the "entrance" barrier of the chemically activated reaction

$$O + CH_3 \rightarrow CH_3O^* \rightarrow H + H_2CO \quad (1a)$$

$$\rightarrow H_2 + HCO \quad (1c)$$

with thermal energies of O and CH_3 added (375 and 387 kJ mol^{-1} at the G2//UMP2 and G2//B3LYP levels, respectively). These values of $\gamma(E)$ result in a 4%−7% branching fraction of the CO-producing channel 1b since the HCO molecule produced in reaction channel 1c is expected to instantly decompose due to the high exothermicity of reaction 1c (354 kJ mol^{-1}) which exceeds the barrier for HCO decomposition (70 kJ mol^{-1}) by a factor of 5 (see section I).

IV.2. Effects of Variations of the Model Parameters−Uncertainty of the Model. Several parameters of the model of reaction 3 have their associated uncertainties, some of which were discussed in section III. In this subsection, effects of variations of these parameters on the final values of γ, the branching ratio of channels 3b and 3a, are investigated with the purpose of assessing the values and sources of the model uncertainties. Calculations were performed with modified G2//UMP2 and CBS-Q//B3LYP models and the resultant values of γ were compared with those obtained using the unmodified versions of the models.

TABLE 3: Properties of Individual Pseudo-Transition States (dividing line segments) and the CH_3O Molecule Used in Calculation of Energy-Dependent Rates and Branching Fractions

i[a]	Δq[b]	E(G2)[c]	E(CBS-Q)[c]	frequency[d]	$\tilde{B}_i \times 10^{-5}$ [e]	B_a[f]	$B_{c,d}$[f]
				UMP2 Surface			
1	0.1950	96.28	92.98	M25	0.175	4.040	1.041
2	0.4578	95.22	91.81	M24	0.032	4.092	1.039
3	0.4173	96.97	93.41	M23	0.038	4.189	1.036
4	0.2541	100.17	96.65	M22	0.103	4.296	1.034
5	0.1738	103.63	100.09	M21	0.220	4.426	1.031
6	0.1340	108.82	105.35	M20	0.371	4.561	1.029
7	0.1115	113.76	110.23	M19	0.535	4.713	1.027
8	0.0983	120.28	117.26	M18	0.688	4.865	1.024
9	0.0643	126.95	123.54	M17	1.611	4.998	1.021
10	0.0352	129.89	126.57	M16	5.369	5.045	1.020
11	0.0352	132.67	129.48	M15	5.361	5.088	1.018
12	0.0361	135.18	132.20	M14	5.109	5.125	1.016
13	0.0381	137.18	134.47	M13	4.589	5.154	1.014
14	0.0416	138.56	136.34	M12	3.846	5.173	1.012
15	0.0524	139.91	138.51	M11	2.428	5.178	1.010
16	0.0473	142.24	141.95	M9	2.970	5.205	1.009
17	0.0584	145.67	146.21	M8	1.950	5.282	1.011
18	0.0524	152.48	153.99	M7	2.424	5.361	1.012
19	0.0497	163.55	165.24	M6	2.694	5.439	1.015
20	0.0485	176.15	177.07	M5	2.826	5.516	1.018
21	0.0477	193.53	193.89	M4	2.931	5.591	1.021
22	0.0467	217.27	217.23	M3	3.051	5.666	1.025
23	0.0456	249.39	249.00	M2	3.198	5.739	1.029
24	0.0450	292.24	291.49	M1	3.280	5.813	1.033
				B3LYP Surface			
1	0.3047	90.65	90.27	D25	0.072	3.402	0.985
2	0.4470	90.76	90.36	D24	0.033	3.527	0.978
3	0.2558	92.93	92.39	D23	0.102	3.629	0.976
4	0.2017	95.70	95.11	D22	0.164	3.738	0.973
5	0.1587	99.24	98.54	D21	0.264	3.863	0.971
6	0.1293	103.54	102.67	D20	0.398	4.000	0.971
7	0.1086	108.44	107.46	D19	0.564	4.136	0.970
8	0.0942	113.98	112.87	D18	0.750	4.277	0.972
9	0.0871	119.81	118.54	D17	0.878	4.407	0.974
10	0.0592	125.63	124.20	D16	1.897	4.536	0.977
11	0.0334	127.52	126.22	D15	5.981	4.576	0.978
12	0.0344	129.12	128.01	D14	5.625	4.611	0.979
13	0.0362	130.37	129.55	D13	5.075	4.642	0.980
14	0.0384	131.40	131.05	D12	4.502	4.668	0.982
15	0.0696	133.01	132.84	D10	1.375	4.717	0.985
16	0.0693	135.24	135.08	D9	1.387	4.794	0.989
17	0.0652	137.63	138.03	D8	1.567	4.873	0.993
18	0.0623	141.86	143.41	D7	1.712	4.941	0.997
19	0.0597	146.44	147.52	D6	1.866	5.019	1.001
20	0.0548	156.23	156.83	D5	2.215	5.087	1.005
21	0.0521	167.03	167.24	D4	2.452	5.154	1.009
22	0.0497	182.41	182.31	D3	2.699	5.220	1.013
23	0.0475	204.18	203.81	D2	2.946	5.287	1.017
24	0.0449	234.31	233.69	D1	3.298	5.353	1.022

Properties of CH_3O

UMP2/6-311G(d,p) frequencies:	821, 990, 1142, 1429, 1432, 1552, 3014, 3094, 3128 cm^{-1}
B3LYP/6-311G(d,p) frequencies:	730, 964, 1108, 1361, 1371, 1518, 2890, 2955, 2996 cm^{-1}
UMP2/6-311G(d,p) rotational constants:	$B_a = 5.264\ cm^{-1}$, $B_{b,c} = 0.9198\ cm^{-1}$
B3LYP/6-311G(d,p) rotational constants:	$B_a = 5.258\ cm^{-1}$, $B_{b,c} = 0.9289\ cm^{-1}$

[a] Number of the pseudo-transition state (segment of the dividing line). Numbers 1−15 (1−14 for the B3LYP surface) represent reaction 3a and numbers 16−24 (15−24 for the B3LYP surface) represent reaction 3b. [b] Width of the corresponding segment of the dividing line in units of Å $amu^{1/2}$. [c] Energy of individual segments calculated with the G2[46] and CBS-Q[47] methods (single-point energy calculations on the UMP2/6-311G(d,p) or B3LYP/6-311G(d,p) optimized surfaces). Energies (in kJ mol^{-1}) are relative to CH_3O and include ZPVE. [d] Numbers of the corresponding points in Tables 1 and 2 upon which the individual segments are centered and whose energies, vibrational frequencies, and rotational constants were used for the calculation of the rate constants (see text,section IV). [e] Rotational constant for pseudorotation (formula XIII) in units of cm^{-1}. [f] Rotational constants of active one-dimensional (B_a) and adiabatic two-dimensional ($B_{c,d} = (B_c B_d)^{1/2}$) rotations in units of cm^{-1}.

Convergence of the results relative to the range of q (coordinate along the PES ridge separating the reactant valley from that of the products) values used was confirmed by performing calculations with one or two of the last segments responsible for the 3b channel omitted. The resultant changes in γ did not exceed 0.4% and 1.6% with one and two last segments removed, respectively. Here and throughout this subsection percentages of changes in γ are given in relative terms (For example, for $\gamma = 0.073$ a relative change of 1.6% means an absolute change of $\delta\gamma = 0.0012$.). Convergence relative to the "step size" in the q coordinate was also established by performing the rate constant calculations with larger steps in q. In these calculations, only every other point among those listed in Tables 1 and 2 was used, twice smaller number of q

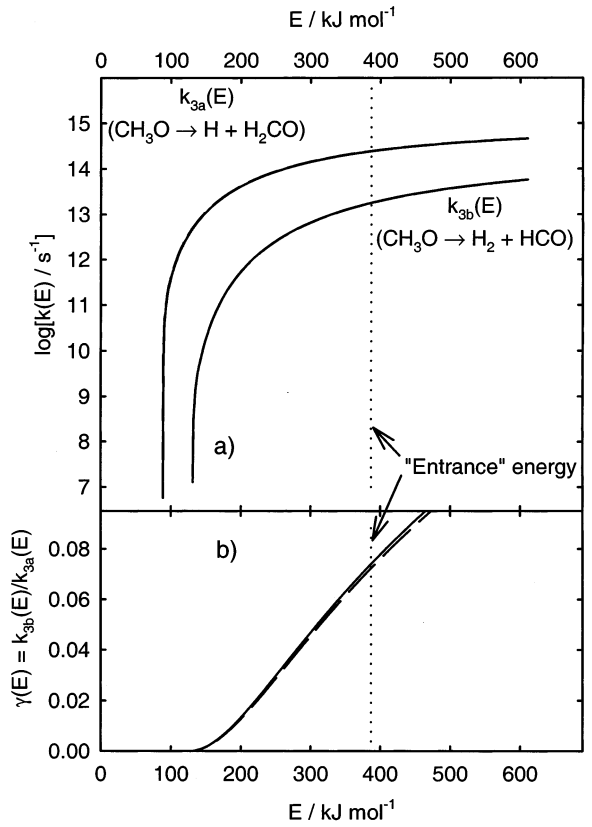

Figure 10. The same as in Figure 9 but obtained using the B3LYP/6-311G(d,p) potential energy surface with G2[46] (solid lines) and CBS-Q[47] (dashed lines) energies calculated along the dividing line (PES ridge).

variable segments was used, and the sizes of the segments were increased accordingly. The changes in γ were +1% for the G2//UMP2 model and −4% for the CBS-Q//B3LYP model.

The effects of the uncertainties associated with the location of the dividing line were investigated by performing rate constant calculations using the alternative "upper" and "lower" dividing lines (see section III). The resultant changes in γ are noticeable but not drastic: +13%(−9%) for the G2//UMP2 model and +10%(−11%) for the CBS-Q//B3LYP model with the "upper"("lower") dividing lines.

The largest effects were those due to the changes in the location of the critical (ridge intersection) point along the dividing line and the changes by a factor of 2 in the questionable frequencies of the "faulty" vibrational modes (see section III). The effects of the changes in the location of the critical point were investigated by assigning one *q* variable segment adjacent to the critical point to the other reactions channel. This means, for the G2//UMP2 model, assigning segment 15 (normally included among those responsible for the reaction channel 3a) to reaction channel 3b, thus increasing the value of γ or, working in the other direction, assigning segment 16 to the reaction channel 3a, thus reducing the value of γ. Such changes in the model are equivalent to changes of the location of the critical point corresponding approximately to the ±0.02 Å change in the HX coordinate in Figures 6 and 7, which covers the area of uncertainty of the location of the intersection of the PES ridges. The resultant changes in γ are +31% (−27%) for the G2//UMP2 model and +13%(−22%) for the CBS-Q//B3LYP model. The effects of the changes by a factor of 2 in the questionable frequencies of the "faulty" vibrational modes were +66% (−22%) for the G2//UMP2 model and +76%(−23%) for the CBS-Q//B3LYP model, where the higher values of γ were obtained with lower values of frequencies and vice versa. For each of the models, cumulative uncertainty equal to a factor of 2 is estimated by converting the above uncertainties expressed as percentages into uncertainty factors, combining the contributions of the three major sources of uncertainties via multiplication, and averaging by taking a geometrical mean.

V. Discussion

V.1. Reactions with Energy Barriers but without Associated PES Saddle Points. This work, to the best of the author's knowledge, is the first attempt to apply a statistical rate theory to quantitatively model reactions that are characterized by energy barriers but have no associated saddle points on the PES. Traditionally, exploration of the mechanisms of chemical reactions via computational methods have concentrated on identification of the PES saddle points and the majority of the mathematical methods of PES analysis developed hitherto serve this purpose. The example of reaction 1c presented in this work demonstrates the importance of reactions without saddle points. One type of reactive system where such "over-the-ridge" reactions can be of significant importance is that of chemically activated reactions with large differences between the "entrance" and the "exit" barriers. In such systems, the energy barrier differences between different channels of decomposition of the adduct can be less important for the competition between these channels than the differences in the entropic (or preexponential) factor. Thus, higher-energy "over-the-ridge" channels may make noticeable contributions.

It is important that methods for identification of "over-the-ridge" reaction channels be developed. In fact, one can always identify a multitude of pathways leading from a particular set of reactants to a particular set of products within the same reactive system. Many of these pathways will be physically unrealistic: proceeding over very high energy barriers or through the areas of coordinate space that correspond to separated fragments. Methods of analysis of the topology of potential energy surfaces that are capable of finding the realistic "over-the-ridge" reaction pathways are needed.

V.2. Uncertainties of the Present Method and Its Application. The uncertainties of the model of reaction 3 developed in this work can be subdivided into those of the method (presented in section II), those of the potential energy surface (section III), and those of the particular procedures used to implement the general method (section IV). The uncertainties of the method arise from the usual assumptions of the RRKM theory (or transition state theory)[9−12] and the additional requirements specific to the current method that one can identify one degree of freedom on the dividing surface that corresponds to the motion along the PES ridge (or the "dividing line") and that its Hamiltonian is separable from that of the rest of the degrees of freedom at each point along the ridge. This additional requirement is not extremely restrictive since local separability of degrees of freedom is usually assumed in practical uses of transition state theory. One more uncertainty of the method is associated with the use of classical rather than quantum treatment of the motion along the PES ridge.

One deficiency inherent to the transition-state-theory-based approach appears in the procedures used to separate the dividing line into the parts responsible for reaction channels 3a and 3b. It is the neglect of the orientation of the momentum vector. A reactive system located to the left of the critical point (Figures 6 and 7) but having a velocity component directed toward valley B is likely to proceed toward the products of channel 3a, H + H_2CO. Similarly, a system crossing the dividing line to the right

of the critical point with a large velocity component oriented toward valley C will continue to the products of the channel 3b, $H_2 + HCO$. Accounting for the orientation of the momentum vector would require a fusion of the dynamical methods with those based on statistical theories of chemical reaction, a desirable development that has not yet been achieved.

The extent of uncertainties originating from the finite accuracy of the potential energy surface can be estimated by comparing the results obtained using the UMP2 and the density functional B3LYP PES and the differences between the $V(q)$ dependences calculated with the G2 and the CBS-Q methods. As can be seen from the plots in Figure 8, both the G2 and the CBS-Q methods give very similar $V(q)$ dependences when used with the same method of geometry optimization. This is reflected in negligible differences between the G2- and CBS-Q-based $k(E)$ and $\gamma(E)$ dependences (Figures 9 and 10). However, the two methods of geometry optimization (UMP2 and B3LYP with the 6-311G-(d,p) basis) result in noticeably different final values of the branching ratio γ of channels 1c and 1a: $\sim$0.04 and $\sim$0.075, respectively. This difference originates, primarily, in the different positions of the critical point on the dividing line (PES ridge) which separates the part of this dividing line corresponding to reaction 3a from that corresponding to reaction 3b. The position of this critical point was identified with the intersection of the three PES ridges: ridge 1 separating the CH_3O valley from $H + CH_2O$, ridge 2 separating $H + CH_2O$ and $H_2 + HCO$, and ridge 3 between the CH_3O and the $H_2 + HCO$ valleys. It was located by analyzing the IRC trajectories started in the vicinities of these three PES ridges. The part of the dividing line responsible for the reaction channel 3b is somewhat larger (the critical point is positioned at a lower value of q) on the B3LYP potential energy surface, which is reflected in the resultant larger γ value.

The issue of the location of this critical point on the dividing line is also related to the uncertainties resulting from the particular procedures used to implement the general method. The method of identification of the critical point based on the analysis of IRC trajectories used in the current work has uncertainties associated with it, as described in section III. The associated variations in the value of γ are described in section IV. It is worth pointing out that the uncertainties of the location of the critical point and the associated variations of γ are less within each of the computational methods used to evaluate the potential energy surface ($\pm$ 0.02 Å in the HX coordinate and 13−31% changes in the γ value) than the 0.0425 Å and 67−80% differences in HX and γ between the results obtained using the UMP2/6-311G(d,p) and the B3LYP/6-311G(d,p) PES.

Finally, the appearance of the second and the third imaginary frequencies among the projected vibrational modes at large values of q (small HX) introduces yet an additional uncertainty in the computed γ values. As was described in section III, the most likely reason for this effect is the influence of the large PES gradient in the direction of the reducing HX values. The remedy used was based on applying relaxed PES scans for the incomplete rotations of the H−X−H moiety corresponding to the vectors of the affected normal modes. The associated uncertainty in γ was estimated by performing rate constant calculations with the affected frequencies increased or decreased by a factor of 2. The effects of varying the frequencies were found to be rather large (22−76%) and comparable with the differences between the results obtained with the UMP2 and the B3LYP surfaces. It can therefore be concluded that development of reliable methods of PES analysis suitable for use in evaluating densities of states on PES ridges is highly desirable.

The applicability of statistical theories of chemical reactions, such as RRKM, to processes that are as fast as the decomposition of the excited CH_3O formed in the $CH_3 + O$ reaction ($k(E) \approx 10^{12}-10^{14}$ s^{-1}) is doubtful. The decomposition of CH_3O^* occurs on a time scale that is too short to allow for full randomization of energy. In this respect, comparing rates of individual channels may still be meaningful although the RRKM formula for $k(E)$ is not valid. Assessment of the relative importance of channels requires only a relaxed ergodicity assumption: that, in the transition states, all states of equal energy are reached with equal probability by the trajectories originating from the excited CH_3O molecule. No assumption of a random energy redistribution within the molecule's phase space is required.

It should be kept in mind when considering the results of the current study that the analysis of the potential energy surface was performed on the basis of two-dimensional relaxed scans in the (HX,XC) coordinate plane. Therefore, although the PES analysis strongly supports the conclusion that the products of the reaction channel 3b are formed without participation of a saddle point, this cannot be decisively assured due to the high dimensionality of the reactive system. The possibility of the existence of a saddle point not found in the current analysis introduces another source of uncertainty, the potential contribution of which cannot be evaluated within the framework of the current analysis.

V.3. Experimental and Calculated Values of the Branching Ratio of Reaction Channels 1b (1c) and 1a. The experimental determinations of the branching fraction of channel 1b were reviewed in the Introduction. The value reported by Seakins and Leone[26] (40 $\pm$ 10%) is in disagreement with that measured by Preses et al.[28] (18 $\pm$ 4%). It appears that the most accurate experimental value of the channel 1b branching fraction is the one obtained recently by Fockenberg[30] in a direct time-resolved laser photolysis/photoionization mass spectrometry study, 15 $\pm$ 3%. The "central model" values of the fraction of channel 1b (originating from the decomposition of HCO produced in channel 1c, see Introduction) calculated in the current work (4% and 7%, depending on the potential energy surface used) are lower than either of the above experimental values. However, the uncertainty range of the current computational study (exemplified by the variations in the branching ratio of up to 76% due to the uncertainties in the vibrational frequencies and up to 27% due to different positioning of the critical point) reaches into the experimental range. In light of the uncertainties of the reaction models used in the calculations (discussed in sections III and IV and in subsection V.2.), the difference between the experimental and the calculated values is not surprising. Considering the fact that a factor of 2−4 differences between the experimental values of entropic (pre-exponential) factors and those derived from quantum chemistry calculations via transition state theory are not unusual for "ordinary" thermal reactions, the current results of modeling of the reaction of the new "over-the-ridge" type can be described as moderately successful. Clearly, further theoretical developments directed at accurate quantitative descriptions of reactions proceeding over energy barriers but not through PES saddle points are needed. The preferred directions of future research can be suggested by the individual factors affecting the uncertainties of calculations, as discussed above in this section.

When this article was under review, the author became aware of another computational study of CO formation in the O +

CH_3 reaction.[51,52] In this work, classical trajectory calculations were used to evaluate the branching fraction of channel 1b and the result coincided with the experimental value of Fockenberg.[30] The authors of ref 51 produced a potential energy surface which is qualitatively similar to the one described in the current study. Analysis of trajectories performed in refs 51 and 52 demonstrated that, among the trajectories responsible for reaction channel 3b (and 1b), there were those passing over the PES ridge 3 (identified as the "transition state" region for the reaction channel 3b in the current study) as well as those passing over ridge 1 and then ridge 2 in a sequence of events characterized by the authors as C−H bond cleavage followed by an abstraction of an H atom from CH_2O. At the same time, trajectories exist that pass over PES ridge 3 but proceed to the H + CH_2O instead of the H_2 + HCO valley.[52] These results illustrate the point made above in the Discussion that a synthesis of dynamics-based and transition state theory-based techniques would be desirable so that the effects of orientation of momentum can be accounted for in selecting the parts of the phase-space separating surface responsible for the individual reaction channels. It is also interesting to note that the branching fraction of the CO-producing channel reported in refs 51 and 52 demonstrates dependence on the total angular momentum J with the $J = 0$ branching fraction (5−10%) being in agreement with the values obtained in the current study (4−7% resulting from the "central models"), which was based on the RRKM formalism without accounting for the angular momentum effects, i.e., also representing the $J = 0$ case. It may be possible that accounting for nonzero angular momentum will change the value of γ. However, such potential effects are not obvious. In the usual implementations of statistical theories of unimolecular reactions, angular momentum influences reaction rates via changes in the effective reaction barrier appearing due to the differences in the two largest (out of three) moments of inertia of the reactant and the transition state. In the reaction considered in the current work, there are almost no differences in the two largest moments of inertia between the transitional structures responsible for the reaction channels 3a and 3b.

VI. Summary

A type of reaction that is characterized by a reaction path proceeding over an energy barrier (a ridge of the potential energy surface) but not through a saddle point is described. A method of computation of rate constants for such "over-the-ridge" reactions is developed on the basis of RRKM and transition state theories. Formulas and computational procedures are presented for the cases of microscopic energy-dependent rates of unimolecular reactions and the thermally averaged rates of unimolecular or bimolecular reactions.

This method was applied to compute the branching fraction of the CO-producing channel (1b) of the reaction of O atom with CH_3 radical. The reaction proceeds through the initial formation of a vibrationally excited CH_3O adduct which decomposes to H + H_2CO (channel 1a) or H_2 + HCO (channel 1c) with subsequent decomposition of HCO due to the large amount of excess energy deposited in the products of reaction 1c:

$$O + CH_3 \rightarrow CH_3O^* \rightarrow H + H_2CO \quad (\Delta H^0_{298} = -286 \text{ kJ mol}^{-1}) \quad (1a)$$

$$\rightarrow H_2 + HCO \quad (\Delta H^0_{298} = -354 \text{ kJ mol}^{-1}) \quad (1c)$$

$$HCO \rightarrow H + CO \quad (2)$$

The sequence of reactions 1c and 2 produce the final products of the experimentally observed reaction channel 1b

$$O + CH_3 \rightarrow H + H_2 + CO \quad (1b)$$

A quantum chemical computational study of the potential energy surface (PES) of the decomposition of CH_3O was performed using the UHF, UMP2, QCISD, and B3LYP methods with the 6-311G(d,p) basis set and with the G2 and the CBS-Q single-point energy calculations. The results demonstrate that the products of reaction channel 1c are formed in a reactive process characterized by trajectories in the coordinate space that proceed over a potential energy ridge but not through a saddle point. Properties of the dividing surfaces associated with the PES ridge and separating the reactant (CH_3O) and products (H + H_2CO and H_2 + HCO) were obtained in quantum chemical calculations. The method developed in this work was used to calculate the microscopic energy-dependent rate constants of the individual channels of decomposition of CH_3O and the branching fraction of the reaction channel 1c (1b). The calculated values of the channel 1c (1b) fraction, 4−7%, depending on the PES used, are lower than the reported experimental results of Preses et al. (18 ± 4%)[28] and Fockenberg (15 ± 3%);[30] however, the ranges of uncertainties of the theoretical and the experimental results overlap.

Acknowledgment. This research was supported by Division of Chemical Sciences, Office of Basic Energy Sciences, Office of Energy Research, U.S. Department of Energy under Grant No. DE/FG02-94ER14463. The author thanks Drs. C. A. Gonzalez and K. K. Irikura for advice and useful discussions and the authors of ref 29 for sharing their results. The author also thanks an anonymous reviewer for the suggestion that the location of the critical point on the dividing line is best termed as an intersection of the PES ridges.

Supporting Information Available: Supplement describing the Z-matrix used in the study of the potential energy surface of reactions 3a and 3b and the values of the variables for selected configurations (Table 1S). This material is available free of charge via the Internet at http://pubs.acs.org.

References and Notes

(1) Valtazanos, P.; Ruedenberg, K. *Theor. Chim. Acta* **1986**, *69*, 281.
(2) Baker, J.; Gill, P. M. W. *J. Comput. Chem.* **1988**, *9*, 465.
(3) Schlegel, H. B. *J. Chem. Soc., Faraday Trans.* **1994**, *90*, 1569.
(4) Taketsugu, T.; Tajima, N.; Hirao, K. *J. Chem. Phys.* **1996**, *105*, 1933.
(5) Yanai, T.; Taketsugu, T.; Hirao, K. *J. Chem. Phys.* **1997**, *107*, 1137.
(6) Quapp, W. *J. Chem. Soc., Faraday Trans.* **1994**, *90*, 1607.
(7) Shaik, S.; Danovich, D.; Sastry, G. N.; Ayala, P. Y.; Schlegel, H. B. *J. Am. Chem. Soc.* **1997**, *119*, 9237.
(8) Preliminary results of the current work were presented at the Second Joint Meeting of the U. S. Sections of the Combustion Institute, Oakland, California, March 2001. Abstract 26.
(9) Gilbert, R. G.; Smith, S. C. *Theory of Unimolecular and Recombination Reactions*; Blackwell: Oxford, 1990.
(10) Holbrook, K. A.; Pilling, M. J.; Robertson, S. H. *Unimolecular Reactions*, 2nd ed.; Wiley: New York, 1996.
(11) Robinson, P. J.; Holbrook, K. A. *Unimolecular Reactions;* Wiley-interscience: New York, 1972.
(12) Forst, W. *Theory of Unimolecular Reactions*; Academic Press: New York, 1973.
(13) Miller, J. A.; Kee, R. J.; Westbrook, C. K. *Annu. Rev. Phys. Chem.* **1990**, *41*, 345.
(14) Warnatz, J. In *Combustion Chemistry*; Gardiner, W. C., Jr., Ed.; Springer-Verlag: New York, 1984.
(15) Warnatz, J.; Mass, U.; Dibble, R. W. *Combustion: Physical and Chemical Fundamentals, Modeling and Simulation, Experiments, Pollutant Formation*; Springer: New York, 1996.
(16) Washida, N. *J. Chem. Phys.* **1980**, *73*, 1665.

(17) Plumb, I. C.; Ryan, K. R. *Int. J. Chem. Kinet.* **1982**, *14*, 861.
(18) Zellner, R.; Hartmann, D.; Karthauser, J.; Rhasa, D.; Weibring, G. *J. Chem. Soc., Faraday Trans. 2* **1988**, *84*, 549.
(19) Slagle, I. R.; Sarzynski, D.; Gutman, D. *J. Phys. Chem.* **1987**, *91*, 4375.
(20) Oser, H.; Walter, D.; Stothard, N. D.; Grotheer, O.; Grotheer, H. H. *Chem. Phys. Lett.* **1991**, *181*, 521.
(21) Lim, K. P.; Michael, J. V. *J. Chem. Phys.* **1993**, *98*, 3919.
(22) Bhaskaran, K. A.; Frank, P.; Just, Th. *Proc. Int. Symp. Shock Tubes Waves* **1980**, *12*, 503.
(23) Fockenberg, C.; Hall, G. E.; Preses, J. M.; Sears, T. J.; Muckerman, J. T. *J. Phys. Chem. A* **1999**, *103*, 5722.
(24) Tsang, W.; Hampson, R. F. *J. Phys. Chem. Ref. Data* **1986**, *15*, 1087.
(25) Baulch, D. L.; Cobos, C. J.; Cox, R. A.; Esser, C.; Frank, P.; Just, Th.; Kerr, J. A.; Pilling, M. J.; Troe, J.; Walker, R. W.; Warnatz, J. *J. Phys. Chem. Ref. Data* **1992**, *21*, 411.
(26) Seakins, P. W.; Leone, S. R. *J. Phys. Chem.* **1992**, *96*, 4478.
(27) Min, Z.; Quandt, R. W.; Wong, T.-H.; Bersohn, R. *J. Chem. Phys.* **1999**, *111*, 7369.
(28) Preses, J. M.; Fockenberg, C.; Flynn, G. W. *J. Phys. Chem.* **2000**, *104*, 6758.
(29) Slagle, I. R.; Kalinovski, I. J.; Gutman, D.; Harding, L. Unpublished manuscript. 1994.
(30) Fockenberg, C. A Kinetics and Product Study of the Reaction of CH_3 Radicals with O(3P) Atoms using Time-Resolved Time-of-Flight Mass Spectrometry. Presented at the 5th International Conference on Chemical Kinetics, National Institute of Standards and Technology, Gaithersburg, Maryland, July 2001. Abstract B4.
(31) Timonen, R. S.; Ratajczak, E.; Gutman, D.; Wagner, A. F. *J. Phys. Chem.* **1987**, *91*, 5325.
(32) Wagner, A. F.; Bowman, J. M. *J. Phys. Chem.* **1987**, *91*, 5314.
(33) Miller, H. W.; Handy, N. C.; Adams, J. E. *J. Chem. Phys.* **1980**, *72*, 99.
(34) Fukui, K. *Acc. Chem. Res.* **1981**, *14*, 363.
(35) Basilevsky, M. V. *Chem. Phys.* **1982**, *67*, 337.
(36) Hoffman, D. K.; Nord, R. S.; Ruedenberg, K. *Theor. Chim. Acta* **1986**, *69*, 265.
(37) Sun, J.-Q.; Ruedenberg, K. *J. Chem. Phys.* **1993**, *98*, 9707.
(38) Heidrich, D.; Kliesch, W.; Quapp, W. *Properties of Chemically Interesting Potential Energy Surfaces. Lecture Notes in Chemistry, Vol. 56*; Springer: Berlin, 1991.
(39) Knyazev, V. D.; Tsang, W. *J. Phys. Chem. A* **1998**, *102*, 9167.
(40) Johnston, H. S. *Gas-Phase Reaction Rate Theory*; The Ronald Press: New York, 1966.
(41) Foresman, J. B.; Frisch, A. E. *Exploring Chemistry With Electronic Structure Methods*, 2nd ed.; Gaussian, Inc.: Pittsburgh, PA, 1996.
(42) Frisch, M. J.; Trucks, G. W.; Schlegel, H. B.; Scuseria, G. E.; Robb, M. A.; Cheeseman, J. R.; Zakrzewski, V. G.; Montgomery, J. A. Jr.; Stratmann, R. E.; Burant, J. C.; Dapprich, S.; Millam, J. M.; Daniels, A. D.; Kudin, K. N.; Strain, M. C.; Farkas, O.; Tomasi, J.; Barone, V.; Cossi, M.; Cammi, R.; Mennucci, B.; Pomelli, C.; Adamo, C.; Clifford, S.; Ochterski, J.; Petersson, G. A.; Ayala, P. Y.; Cui, Q.; Morokuma, K.; Malick, D. K.; Rabuck, A. D.; Raghavachari, K.; Foresman, J. B.; Cioslowski, J.; Ortiz, J. V.; Baboul, A. G.; Stefanov, B. B.; Liu, G.; Liashenko, A.; Piskorz, P.; Komaromi, I.; Gomperts, R.; Martin, R. L.; Fox, D. J.; Keith, T.; Al-Laham, M. A.; Peng, C. Y.; Nanayakkara, A.; Gonzalez, C.; Challacombe, M.; Gill, P. M. W.; Johnson, B.; Chen, W.; Wong, M. W.; Andres, J. L.; Gonzalez, C.; Head-Gordon, M.; Replogle, E. S.; Pople, J. A. *Gaussian 98*, revision A.7; Gaussian, Inc.: Pittsburgh, PA, 1998.
(43) Certain commercial instruments and materials are identified in this article to adequately specify the procedures. In no case does such identification imply recommendation or endorsement by NIST, nor does it imply that the instruments or materials are necessarily the best available for these purposes.
(44) ter Horst, M. A.; Schatz, G. C.; Harding, L. B. *J. Chem. Phys.* **1996**, *105*, 558.
(45) Gonzalez, C.; Schlegel, H. B. *J. Phys. Chem.* **1990**, *94*, 5523.
(46) Curtiss, L. A.; Raghavachari, K.; Trucks, G. W.; Pople, J. A. *J. Chem. Phys.* **1991**, *94*, 7221.
(47) Ochterski, J. W.; Petersson, G. A.; Montgomery, J. A. *J. Chem. Phys.***1996**, *104*, 2598.
(48) Baboul, A. G.; Schlegel, H. B. *J. Chem. Phys.* **1997**, *107*, 9413.
(49) Pechukas, P. *Dynamics of Molecular Collisions*; Miller, W. H., Ed.; Plenum Press: New York, 1976; Vol. Part B.
(50) Karas, A. J.; Gilbert, R. G.; Collins, M. A. *Chem. Phys. Lett.* **1992**, *193*, 181.
(51) Marcy, T. P.; Diaz, R. R.; Heard, D.; Leone, S. R.; Harding, L. B.; Klippenstein, S. J. *J. Phys. Chem. A* **2001**, *105*, 8361.
(52) Harding, L. B. Radical−Radical Recombination Reactions: O + CH_3. Presented at the 5th International Conference on Chemical Kinetics, National Institute of Standards and Technology, Gaithersburg, Maryland, July 2001. Abstract B1.